Bulk and surface vibrational modes in NiAl

Mark Mostoller, R. M. Nicklow, and D. M. Zehner
Solid State Division, Oak Ridge National Laboratory, P.O. Box 2008, Oak Ridge, Tennessee 37831-6032

S.-C. Lui,* J. M. Mundenar,† and E. W. Plummer
Department of Physics and Laboratory for Research on the Structure of Matter, University of Pennsylvania, Philadelphia, Pennsylvania 19104

(Received 23 January 1989)

We have measured the phonon dispersion curves of bulk NiAl along the three major symmetry directions by neutron scattering, and fitted the results with force models extending to third- and fourth-nearest neighbors. Our electron-energy-loss experiments show that dipole-active vibrational modes occur in the gap between the bulk acoustical and optical modes for the (110) and (111) surfaces. We have done extensive slab calculations of the vibrational modes at the surface-Brillouin-zone center for these two faces and for NiAl(001). The calculations indicate that the atomic motion for the gap modes is correlated with the bulk properties. Adjustment of the interplanar force constants in directions intuitively consistent with experimental results for the surface relaxations can shift the calculated frequencies into agreement with experiment.

I. INTRODUCTION

Lattice vibrations in bulk solids and at solid surfaces can be studied experimentally in a variety of ways. In the bulk, by far the most useful technique is coherent inelastic neutron scattering, because it allows direct measurement of the phonon dispersion curves; that is, measurement of the phonon frequencies as a function of wave vector. The dispersion curves can in turn be used to determine the interatomic forces in the solid. Neutron-scattering studies of most elemental metals were done from the early 1960s to the mid 1970s. In 1961, for example, Brockhouse *et al.* measured the phonon dispersion curves of lead[1] and reported perhaps the first direct observation of Kohn anomalies in their results. Directly or indirectly relevant to the present work, other monatomic metals whose phonon spectra have been studied by neutron scattering include nickel,[2] aluminum,[3,4] iron,[5,6] copper,[7–9] and zinc.[10]

Neutron-scattering experiments have also been performed on a large number of ordered metal alloys. Among the earliest was the work of Gilat and Dolling on β-brass (CuZn).[11] Smith and Gläser looked at the transition-metal carbides NbC, TaC, and HfC,[12] in which the large difference in the atomic masses of the metal and carbon atoms produces a gap between the acoustic and optic modes. Nickel-aluminum alloys have been investigated heretofore: Stassis *et al.*[13] have measured the phonon spectra of Ni_3Al, which has a rather small gap of about 0.7 THz, and Shapiro *et al.*[14] have studied Kohn-like anomalies in one of the transverse-acoustic branches of $Ni_{0.5+x}Al_{0.5-x}$ along the [110] direction.

Two methods have proven to be especially useful in the study of surface vibrations. One is the inelastic scattering of helium atoms. For example, Brusdeylins *et al.*[15] have measured the dispersion of the Rayleigh surface phonon of LiF(001) by helium-atom scattering. For W(001), Ernst *et al.*[16] observed not only the Rayleigh wave along the [110] direction, but also an anomalous mode whose frequency became very small near the boundary of the surface Brillouin zone. As the temperature was reduced, this mode softened still further, indicating that the well-known $\sqrt{2}\times\sqrt{2}$ reconstruction of W(001) may be a continuous displacive transition driven by this soft mode.

The other method is electron-energy-loss spectroscopy (EELS), which has been in use longer and is the technique employed in the present work. For metals, as the resolution, sensitivity, and impact energy range of the EELS technique have improved, a variety of clean and adsorbate-covered surfaces have been investigated.[17] For clean surfaces of elemental metals, for example, there have been the observation of high-frequency surface states above the bulk phonon bands at a stepped Pt(111) surface,[18] measurement of the dispersion of the Rayleigh wave on Ni(001) (Ref. 19) and Cu(001) (Ref. 20) and of several surface modes at Cu(111),[21] and the observation of surface resonant modes for Cu(110), Ni(110), and Fe(111) at frequencies where the surface-projected bulk spectral density is small.[22,23]

Surface vibrations of a few ordered metal alloys have recently been studied with EELS. In a very nice series of papers, Oshima and collaborators reported the dispersion of a rich variety of true surface states and surface resonant modes at the (001) surfaces of the superconducting transition-metal carbides NbC and TaC, and the related, nonsuperconducting compound HfC.[24–26] Surface vibrations at the (001) and the stepped (310) faces of TiC have also been investigated by this group.[27,28] One of the features of the results reported for the carbides is the appearance of surface states in the gap between the bulk acoustical and optical bands.

When a crystal is cleaved to form a surface, this intro-

duces an extremely severe perturbation of the electronic and vibrational structure. At the simplest level, the atomic coordination changes; atoms in the surface region have fewer neighbors, and as a result may be intuitively expected to be more loosely bound and to perhaps vibrate at lower frequencies. In materials with a gap between optic and acoustic modes in the bulk, the severe perturbation represented by cleavage might be expected to drive some modes down out of the optic band to form surface states in the gap, as does occur for the carbides. The Rayleigh wave is a surface acoustical vibration that splits off below the corresponding acoustic mode of the bulk.

At the surface, the atoms relax to different interplanar spacings normal to the surface (and in many cases also reconstruct into two-dimensional lattices of lower symmetry parallel to the surface). In virtually any model based on pair potentials or chemical-bonding arguments, the reduction in coordination at the surface would lead one to expect outward relaxation. In fact, for most metals, the opposite occurs: the relaxation is generally inward. Finnis and Heine[29] explained this qualitatively by noting that the electrons at the surface would smooth out rather than remain frozen in their bulk distribution, resulting in a net inward electrostatic force on the metal surface ions. Landman, Hill, and Mostoller[30] later showed that the magnitudes and trends in the relaxations predicted by this electrostatic effect were consistent with experimental results and, furthermore, that significant relaxation might be expected to extend several layers deep in some cases. With atomic relaxation and electronic redistribution, changes in the interatomic forces in the surface region will occur. These changes may shift the frequencies of predicted surface states or resonances, eliminate them, or give rise to new ones.

In this paper, we report measurements of the bulk phonon spectra of NiAl by coherent inelastic neutron scattering, and of the dipole-active surface vibrations at the center of the surface Brillouin zone for the (110) and (111) surfaces by EELS. The results are interpreted in terms of interatomic force models extending to third- or fourth-nearest neighbors and slab calculations incorporating changes in the largest interatomic forces. The calculations also predict a gap mode for the (001) surface, and its frequency is estimated from the measured change in bond length. The decay patterns for the atomic displacements in the surface modes are strongly influenced by the bulk phonon properties.

NiAl is an attractive candidate for study for several reasons. The mass ratio is greater than 2, making it likely that there will be a gap in the bulk phonon spectra. Sufficiently large single crystals can be grown that inelastic neutron scattering can be used to determine the bulk phonon spectrum. The low-Miller-index surfaces have been investigated by several surface techniques, including low-energy electron diffraction (LEED),[31–34] photoemission,[35] medium-energy ion scattering (MEIS),[36] and low-energy ion scattering (LEIS).[37,38] The (110) and (111) surfaces are particularly interesting because the former is rumpled[31,32,36,37] while, for the latter, LEED analysis[33] and LEIS (Ref. 38) suggest the presence of roughly equal areas of both Ni-terminated and Al-terminated domains.

Elemental Ni and Al, and the ordered alloys NiAl and Ni_3Al, are all cubic metals: Ni and Al have the fcc structure, NiAl the bcc-like CsCl structure, and Ni_3Al the fcc-like $L1_2$ structure, with Al at the cube corners and Ni at the face centers. These materials offer the opportunity to study metallic bonding and interatomic forces, both in the bulk and at surfaces, in a family of structurally simple systems. The chemistry of the various surfaces of NiAl differs from face to face. In addition, NiAl has been identified as a candidate material for making stable epitaxial contacts to III-V compound semiconductors.[39,40]

The structure of the paper is as follows. In Sec. II, the measurements and interpretation of the bulk phonons are presented. Section III reports the experimental and theoretical results for the surface vibrations. Conclusions are briefly summarized in Sec. IV.

II. BULK VIBRATIONS

The bulk phonon dispersion curves of NiAl were measured using the HB-3 triple-axis neutron spectrometer at the High Flux Isotope Reactor at the Oak Ridge National Laboratory. The data were obtained with the spectrometer operating in the standard constant-Q mode, where Q denotes the neutron-scattering wave vector, and with the final neutron energy E_f also held constant. Various values for E_f in the 6–10 THz range were used in order to optimize compromises between intensity and resolution for each branch, and to facilitate identification of spurious signals due to harmonic wavelength contamination as the beam could not be filtered for many of the measurements. For most of the measurements, the (0002) planes of Be crystals were used for the monochromator and analyzer. The beam collimation was typically reactor-60′-monochromator-40′-sample-40′-analyzer-300′-detector.

The NiAl single-crystal sample had a volume of approximately 0.73 cm^3, and its stoichiometry was determined to be 50.6 ± 2 % Al by Paschen optical-emission spectroscopy and the use of standard solutions. In addition, spark-source mass spectroscopy was invoked to ensure that there were no major impurities in the sample (total $<$ 100 ppm weight concentration). For most of the measurements, the sample was oriented with a (110)-type mirror plane parallel to the (horizontal) scattering plane of the spectrometer. With this geometry, all of the phonon modes propagating along the [001] and [111] directions could be observed, as well as the longitudinal and the higher-frequency transverse modes along [110]. The lower-frequency TA_1[110] modes were observed with the sample oriented to have a (001)-type mirror plane horizontal.

The measured phonon frequencies are listed in Table I and shown as symbols in Figs. 1 and 2. Table I also gives the estimated experimental uncertainties. Since surface excitation energies are typically given in eV or meV, we note here that 1 THz$=$4.135 meV.

The interatomic force constants of a conventional Born–von Kármán model extending as far as third- or fourth-nearest neighbors (3NN or 4NN) were determined by a least-squares fit to the data. In such fits, it is cus-

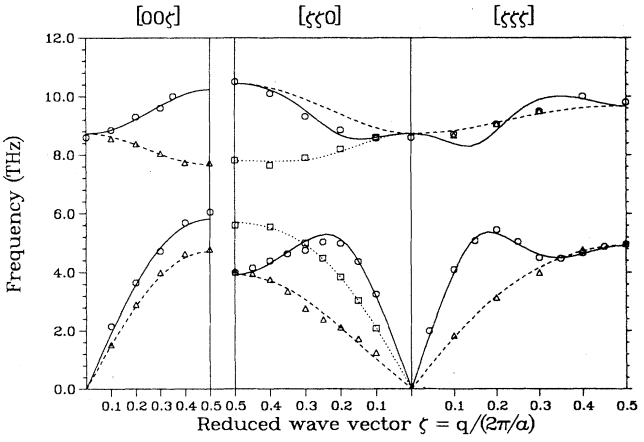

FIG. 1. Calculated (4NN) and experimental dispersion curves for NiAl. Solid lines and circles represent the longitudinal modes, dashed lines and triangles the transverse modes. Along the [110] direction, the dashed lines and triangles are the T_1 modes, in which the atoms vibrate along $(1\bar{1}0)$, and the dotted lines and squares are the T_2 modes, in which the atoms vibrate along (001).

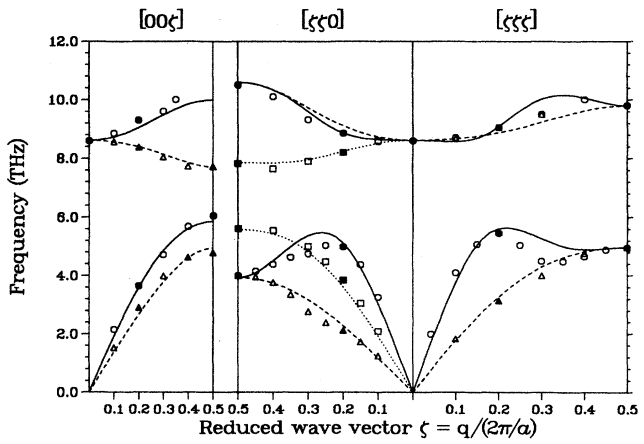

FIG. 2. Calculated (3NN) and experimental dispersion curves for NiAl. The solid symbols are the experimental data points to which the 3NN model was fitted.

TABLE I. Measured normal-mode frequencies (THz) in NiAl at 296 K. The polarization vectors for the TO_1, TA_1 and TO_2, TA_2 modes along the [ζζ0] direction are parallel to $[1\bar{1}0]$ and [001], respectively.

[00ζ]	LO	TO		LA	TA	
0.0	8.60±0.08					
0.10	8.85±0.10	8.56±0.10		2.15±0.02	1.52±0.02	
0.20	9.30±0.10	8.38±0.10		3.65±0.03	2.90±0.02	
0.30	9.60±0.10	8.05±0.10		4.72±0.02	3.99±0.02	
0.35	10.00±0.20					
0.40		7.73±0.06		5.68±0.03	4.63±0.03	
0.50		7.72±0.10		6.05±0.05	4.78±0.03	
[ζζ0]	LO	TO_1	TO_2	LA	TA_1	TA_2
0.0	8.60±0.08					
0.10	8.57±0.10		8.61±0.10	3.26±0.02	1.24±0.01	2.09±0.01
0.15				4.37±0.02	1.72±0.01	3.05±0.01
0.20	8.85±0.10		8.20±0.10	4.98±0.03	2.12±0.01	3.84±0.04
0.25				5.04±0.03	2.39±0.01	4.48±0.01
0.30	9.32±0.10		7.90±0.10	4.75±0.03	2.76±0.01	5.00±0.04
0.35				4.63±0.03	3.35±0.01	
0.40	10.10±0.10		7.65±0.10	4.39±0.04	3.76±0.02	5.55±0.04
0.45				4.15±0.04	3.95±0.03	
0.50	10.50±0.10		7.82±0.20	4.00±0.04	4.00±0.04	5.60±0.05
[ζζζ]	LO	TO		LA	TA	
0.042				2.00±0.02		
0.10	8.71±0.10	8.68±0.10		4.10±0.10	1.83±0.03	
0.15				5.07±0.04		
0.20	9.05±0.10	9.05±0.10		5.45±0.04	3.14±0.02	
0.25				5.05±0.02		
0.30	9.50±0.10	9.50±0.10		4.50±0.02	4.00±0.10	
0.35				4.48±0.02		
0.40	10.00±0.10			4.65±0.02	4.76±0.02	
0.45				4.88±0.02		
0.50	9.80±0.20			4.96±0.02	4.96±0.02	

tomary to weight the differences between the calculated and observed frequencies with the inverse of the experimental errors,[41] that is, to minimize χ as defined by

$$\chi^2=\frac{1}{N-K}\sum_{i=1}^{N}\left[\frac{\Delta\nu_i}{\sigma_i}\right]^2, \quad (1)$$

where N is the number of frequencies fitted, K is the number of adjustable parameters, and σ_i is the error for the ith phonon. Another measure of the overall quality of the fit is the standard error S, defined like χ but without the weighting,

$$S^2=\frac{1}{N-K}\sum_{i=1}^{N}(\Delta\nu_i)^2 . \quad (2)$$

Inspection of Table I shows that there is nearly twice as much data for the acoustic modes as for the optic modes and, furthermore, that the errors are generally much smaller for the acoustic modes. A weighted fit would therefore largely ignore the optic modes. To avoid this, we therefore chose to do an unweighted fit, that is, to minimize the standard error.

To obtain a quantitatively satisfactory fit to the data, it is necessary to include interactions through 4NN's. The parameters of a 4NN model are given in Table II, and the calculated dispersion curves of this model are shown with the data in Fig. 1. The calculations are in generally good agreement with the data, except that they do not reproduce the depression in the $TA_1[110]$ mode around $\zeta\sim0.25$. We will discuss this anomaly in the measured dispersion curves later on.

For the purposes of the slab calculations of surface phonons to be discussed in Sec. III, including 4NN interactions adds significantly to the algebraic and computational burden. For those calculations we therefore chose to use a 3NN model fitted to the data at seven wave vectors, namely $q=0$, the three zone-boundary points, and one interior point along each direction. We fitted only these selected data to try to best reproduce the observed gaps. The parameters of this 3NN model are given in Table II (the value for S in the table is for all the data, not just for the frequencies at the seven selected wave vectors), and the 3NN dispersion curves are compared to the data in Fig. 2. The fit is clearly not as good as that of the 4NN model, especially for the dip in the LA[111] mode, but it is quantatively reasonable and there is good agreement with the gaps between corresponding acoustical and optical modes along the three directions.

Referring to Fig. 2, the observed anomaly in the $TA_1[110]$ mode is a dip below "normal" behavior for wave vectors $\zeta\sim0.15$–0.40, with the maximum deviation at $\zeta\sim0.28$. Shapiro *et al.*[14] have studied this anomaly as a function of concentration in Ni_xAl_{1-x} for $x=0.50$, 0.58, and 0.63. The anomaly shifts linearly to lower wave vectors with increasing x, but remains roughly the same in magnitude. This is accompanied by a decrease in the elastic constant $c'=(c_{11}-c_{12})/2$; that is, in the slope of this mode at $q=0$.

In the mode in question, the atoms vibrate along the $(1\bar{1}0)$ direction transverse to the [110] direction of propagation. As discussed by Shapiro *et al.*, this correlates with precursor effects of a tetragonal martensitic transformation observed above the transformation temperature T_M. These precursor effects are tweedlike striations in transmission-electron-microscope images, and [110] ridges of diffuse scattering in electron-diffraction patterns and in elastic neutron-scattering spectra. They are taken as evidence of embryos of a tetragonally distorted second phase with static distortions along $(1\bar{1}0)$. All the precursor effects become more pronounced as the temperature is reduced toward T_M, which itself rises with increasing nickel concentration. Shapiro *et al.* suggest that both the static effects and the phonon anomaly may have a common origin in the electron-ion coupling for scattering near the Fermi surface.

Connally and Johnson[42] have calculated the electronic band structure of stoichiometric NiAl, using the nonrelativistic augmented-plane-wave (APW) method supplemented by linear combination of atomic orbitals (LCAO) interpolation. While they do not show the Fermi surface, the energy bands appear to have have hole pockets centered at $R=(\frac{1}{2},\frac{1}{2},\frac{1}{2})$ that are spanned by the reduced wave vectors $\zeta\sim0.26$ and 0.29. More recently, Nagel[43] has done APW calculations of the electronic band structure of FeAl, CoAl, and NiAl. His Fermi-surface cross sections for NiAl clarify the structure around R; they show a hole surface spanned by $\zeta\sim0.29$ and an empty portion of an electron "jungle gym" surface spanned by $\zeta\sim0.32$. These values correspond well with the position of the observed phonon anomaly. In a rigid-band picture, increasing the nickel concentration would add electrons, raise the Fermi energy, and cause these pockets to

TABLE II. Interatomic force constants (dyn/cm) for a 4NN Born–von Kármán model fitted to all of the measured frequencies in Table I, and for a 3NN model fitted to the data at seven selected wave vectors; in reduced units, these seven wave vectors are (0,0,0), (0,0,0.2), (0,0,0.5), (0.2,0.2,0), (0.5,0.5,0), (0.2,0.2,0.2), (0.5,0.5,0.5).

		r (Å)	4NN model	3NN model
Ni-Al	(111,xx)	2.500	10440	11240
	(111,xy)		10680	10090
Ni-Ni	(200,xx)	2.887	780	2180
	(200,zz)		−280	−440
Al-Al	(200,xx)		18820	18380
	(200,zz)		−280	760
Ni-Ni	(220,xx)	4.083	2160	2070
	(220,zz)		−2910	−1370
	(220,xy)		2140	2690
Al-Al	(220,xx)		1100	820
	(220,zz)		510	710
	(220,xy)		1180	2760
Ni-Al	(311,xx)	4.788	−70	
	(311,yy)		590	
	(311,yz)		−640	
	(311,xy)		850	
S			0.147	0.246

shrink. This in turn would move any associated structure at $q=2k_F$ down in q, as is observed for the phonon anomaly by Shapiro *et al.* It should be noted that this is somewhat speculative; establishing a connection between phonon anomalies and electronic structure requires detailed calculations that include the electron-phonon matrix elements.[44]

Figure 3 shows the density of states for NiAl calculated from the 4NN model. The gap between acoustic and optic modes is 1.84 THz (7.6 meV) wide, from 5.82 to 7.66 THz (24.1–31.7 meV). Projected densities of states for vibrations of Ni and Al were also calculated. Although these are not shown, they indicate that the acoustic modes, the states below the gap in Figs. 1–3, are almost entirely vibrations of the heavier Ni atoms, and the optic modes are predominantly vibrations of the lighter Al atoms. The calculated rms amplitudes of vibration of Ni and Al are comparable over the range $T=0-500$ K, but the Debye temperatures corresponding to these rms displacements are quite different: at room temperature, $\Theta_D(\mathrm{Ni})=332$ K and $\Theta_D(\mathrm{Al})=563$ K.[45] The rms vibrational amplitudes were among the quantities varied by Yalisove and Graham[36] to fit the data in their MEIS study of the rippling of the NiAl surface. They found equal bulk rms amplitudes for Ni and Al, and Debye temperatures $\Theta_D(\mathrm{Ni})=345$ K and $\Theta_D(\mathrm{Al})=520$ K, in good agreement with our values.

While it might at first seem surprising that the rms vibrational amplitudes for the two components of a binary compound are comparable over a broad temperature range, this is in fact not unusual. For cubic crystals, it is fairly straightforward to derive the following low- and high-temperature limits for the mean-square amplitude for b atoms along the (for cubic crystals arbitrary) direction α:

$$\langle u_\alpha^2(T,b)\rangle = \begin{cases} \dfrac{h}{3M_b}\left\langle \dfrac{1}{\omega}\right\rangle_b & \text{as } T\to 0 \\ \dfrac{kT}{3M_b}\left\langle \dfrac{1}{\omega^2}\right\rangle_b & \text{as } T\to\infty \end{cases},$$

where $\langle 1/\omega^n\rangle_b$ is the nth inverse frequency moment of the density of states for b atoms. The rms displacements therefore give the most weight to the lowest-frequency portion of the spectrum, the acoustic modes, in which the atoms vibrate in phase. If the atoms vibrated in phase throughout the zone, the rms amplitudes would be the same to all temperatures.

To compare our results for NiAl with those for other materials, we did calculations for two alloys (CuZn and KCl) with mass ratios near 1, two (NiAl and KBr) with ratios of about 2, and one (TaC) with a mass ratio of 15. In every case, the rms amplitudes of the two constituents were within 15% of one another at 50 and 500 K, except for TaC at 50 K, where $\langle u_\alpha^2(\mathrm{C})\rangle^{1/2}\sim 2\langle u_\alpha^2(\mathrm{Ta})\rangle^{1/2}$.

The lattice dynamics of pure Ni (Ref. 2) and Al (Refs. 3 and 4) and of the ordered compounds NiAl and Ni_3Al (Ref. 13) have all now been measured and analyzed in terms of Born–von Kármán models. Ni and Al have the fcc structure, NiAl the bcc-like CsCl structure, and

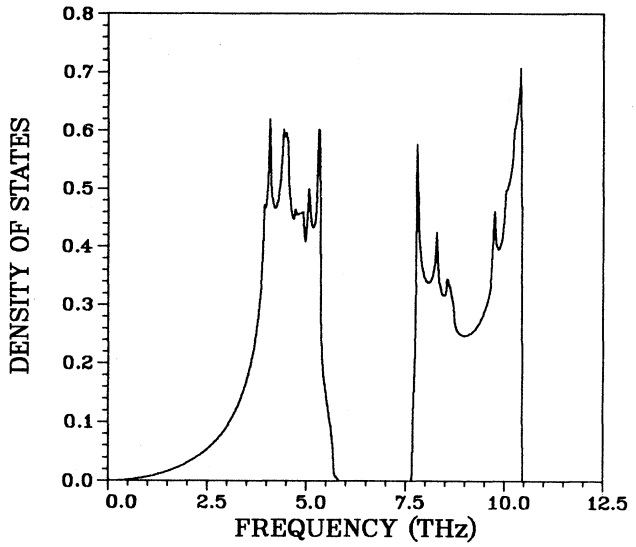

FIG. 3. Phonon density of states for NiAl calculated from the 4NN model.

Ni_3Al the fcc-like $L1_2$ (Cu_3Au) structure, with Al at the cube corners and Ni at the face centers. It is of interest to see if there are any correlations among the interatomic distances and forces in this family of metals.

Table III lists interatomic distances in these materials, and the radial (bond-stretching) force constants for the first few neighbor pairs. It is evident that the first three Al-Al neighbor distances are nearly the same in Al and NiAl, and that the 1NN and 2NN Al-Al force constants are comparable in the two materials. In Ni and Ni_3Al, the first four Ni-Ni distances and the 1NN Ni-Ni force constant are very similar. NiAl is like simple-cubic Al with the same 1NN-3NN distances as in fcc Al, and with interstitial Ni atoms at the body centers. Ni_3Al appears to be like Ni with substitutional Al atoms placed so that the Al-Al separations are much larger than the 1NN separation in pure Al. The only distance in the compounds that appears to be out of place, in the sense that there is no corresponding distance in the elemental metals, is the 4NN Ni-Al separation in NiAl.

Another, smaller family of metals for which information on the lattice dynamics is available is α-Fe,[6] Al, and Fe_3Al.[6] α-Fe has the bcc structure, Al is fcc and Fe_3Al has the bcc-like $D0_3$ structure in which the Al atoms occupy alternate cube corners along the curve edges. Table IV gives the interatomic distances and force constants for these three metals. In this case, the first five Fe-Fe distances in Fe_3Al are only slightly larger than in α-Fe, and the 1NN Fe-Fe force constant is comparable in the elemental metal and the compound. The first two Al-Al distances in the compound are about 1% larger than the 2NN and 3NN separations in pure Al. Fe_3Al is essentially bcc Fe with substitutional Al atoms at alternate cube corners.

Finally, the lattice dynamics of Cu,[7–9] Zn,[10,46,47] and CuZn [β-brass (Ref. 11)] have also been measured and analyzed some years ago. The 3d transition metals Cu and Zn are adjacent in the Periodic Table, and both have

TABLE III. Interatomic distances r (Å) and radial force constants A (dyn/cm) in Ni, Al, and in the ordered compounds NiAl and Ni_3Al. Here, the radial force constants for various neighbor directions are defined as follows: $A(m00)=(m00;xx)$, $A(mm0)=(mm0;xx)+(mm0;xy)$, and $A(mmm)=(mmm;xx)+2(mmm;xy)$. The second row of the table gives the crystal structure.

Ni[a] fcc $a=3.524$		Al[b] fcc $a=4.041$		NiAl[c] CsCl $a=2.887$			Ni_3Al[d] $L1_2$ $a=3.568$		
r	A	r	A	r	A	Pair	r	A	Pair
2.49	36 490			2.50	31 800	Ni-Al	2.52	35 260	Ni-Ni
								19 130	Ni-Al
		2.86	21 230	2.89	18 820	Al-Al			
					780	Ni-Ni			
3.52	880						3.57	6740	Ni-Ni
								−2130	Al-Al
		4.05	2490	4.08	2280	Al-Al			
					4300	Ni-Ni			
4.32							4.37		Ni-Ni
									Ni-Al
				4.79		Ni-Al			
4.98		4.95		5.00		Al-Al	5.05		Ni-Ni
						Ni-Ni			Al-Al

[a]Reference 2, model (a).
[b]Reference 3.
[c]Present work, 4NN model.
[d]Reference 13.

close-packed structures; Cu is fcc, and Zn is hcp with a much larger c/a ratio of 1.86 than the ideal hcp value of 1.63. CuZn has the CsCl structure. Table V lists distances and force constants for these materials. The 1NN force constants and distances are similar for the three, and the 2NN distances in Zn and CuZn are roughly the same. Beyond that, however, there is no correlation in interatomic distances like that which occurs for the two other families.

For the three ordered alloys involving the simple metal Al, there is a rather striking correspondence between the interatomic distances in the elemental metals and those in the compounds. In addition, the first-neighbor force constants in the elemental metals could have served as good first estimates of the corresponding interactions in the alloys.

TABLE IV. Interatomic distances r (Å) and radial force constants A (dyn/cm) in α-Fe, Al, and in the ordered compound Fe_3Al.

Fe[a] bcc $a=2.860$		Al[b] fcc $a=4.041$		Fe_3Al[a] DO_3 $a=5.792$		
r	A	r	A	r	A	Pair
2.48	47 680			2.51	43 540	Fe-Fe
					56 470	Fe-Al
2.86	14 920	2.86	21 230	2.90	3050	Fe-Fe
					11 130	Fe-Al
4.04	1540	4.05	2490	4.10	3920	Fe-Fe
					3020	Fe-Fe
					520	Al-Al
4.74				4.80		Fe-Fe
						Fe-Al
4.95		4.95		5.02		Fe-Fe
						Al-Al

[a]Reference 6, model 2 for Fe_3Al.
[b]Reference 3.

TABLE V. Interatomic distances r (Å) and radial force constants A (dyn/cm) in Cu, Zn, and in the ordered compound CuZn (β-brass).

Cu[a] fcc $a=3.608$		Zn[b,c] bcc $a=2.6648$ $c=4.9467$		CuZn[d] CsCl $a=2.945$		
r	A	r	A	r	A	Pair
2.55	27 750	2.66	24 420 27 800	2.55	31 100	Cu-Zn
		2.91	7300 7600	2.95	7110 730	Cu-Cu Zn-Zn
3.61	530					
		3.95	3700 4800	4.16	1070 1190	Cu-Cu Zn-Zn
4.42						
		4.76		4.88		Cu-Zn
5.10		4.95		5.10		Zn-Zn Cu-Cu

[a]Reference 9, 298 K.
[b]Reference 46, average radial force constant $(2K+C_{Bx}+C_{Bz})/2$ in the notation of these authors.
[c]Reference 47, model B, average radial force constant as above.
[d]Reference 11.

III. SURFACE VIBRATIONS

A. Experiment

Samples for measurements of surface vibrations and electronic structure were cut from the same single crystal used to study the bulk phonon dispersion curves. Electron-energy-loss spectroscopy (EELS) was used to search for dipole-active surface vibrational modes. The measurements were performed at the University of Pennsylvania with a Leybold-Heraeus model ELS-22 spectrometer in an ultrahigh-vacuum chamber with a base pressure of 7×10^{-11} Torr. Spectra were recorded in the specular direction with an incident angle of 60° with respect to the surface normal. Any vibrational loss peaks observed will correspond to vibrations normal to the surface for two-dimensional wave vectors at the Γ point, that is, at the center of the surface Brillouin zone (SBZ). The electron impact energies were 1.5 and 2.7 eV for the (110) and (111) surfaces, respectively. Unfortunately, the spectrometer could not maintain adequate energy resolution at input energies required for dispersion measurements.

The details of sample preparation and characterization have been reported previously.[31,35,48] Briefly, the samples were cut to expose the three low-index faces and mechanically polished. In the vacuum chamber, the surfaces were cleaned by cycles of Ne^+ ion sputtering followed by annealing to 800–1000 °C. This procedure gave clean, well-ordered surfaces as attested by sharp 1×1 LEED patterns. The surfaces, as in previous studies, were free of contaminants (S,O,C), and the Ni:Al ratio at the diatomic (110) surface is expected to be 1:1 as in the bulk.[31]

In addition to the work to be presented for the (110) and (111) surfaces, a NiAl(001) sample was examined. We have been unable to repeatedly observe losses associated with surface vibrations at this face. Difficulties occurred with tuning the spectrometer for this surface. Furthermore, reproducible surface preparation proved difficult. Specifically, in investigating how to clean this face, it was determined that subsequent to annealing the sputtered surface to ~700 °C, the LEED pattern revealed a $c(3\sqrt{2}\times\sqrt{2})R45°$ reconstruction. For freshly polished surfaces, a (1×1) pattern was observed after annealing to ~1000 °C. However, after repeated cleaning cycles it became impossible to prepare surfaces which did not contain some regions of reconstruction. In subsequent LEIS studies of a different NiAl(001) sample, Mullins and Overbury[37] concluded that the outermost layer in both structures is a mixture of (predominantly) Al and Ni atoms, and that the (1×1) surface is disordered.

EELS spectra recorded at room temperature are shown in Fig. 4 for the (110) and (111) faces. For the (110) surface, there is a relatively strong loss peak at 27 meV (6.53 THz), while for (111), there is a weaker peak at 31 meV (7.50 THz). Spectra obtained in an off-specular geometry confirmed that the (110) mode is dipole active, but as a result of contamination problems to be discussed shortly, it was not possible to obtain off-specular data for the (111) face. The surface phonon peak for the (110) surface is roughly 4 times stronger than that for (111), indicating that the induced dipole for the former is much larger. An additional peak can be seen at ~55 meV in the (111) spectrum that we attribute to the C—M stretch of adsorbed CO. In contrast to the far less reactive (110) surface, it was not possible to clean the (111) surface and acquire a spectrum before a detectable amount of CO was present. In their study of S, CO, and O adsorption on

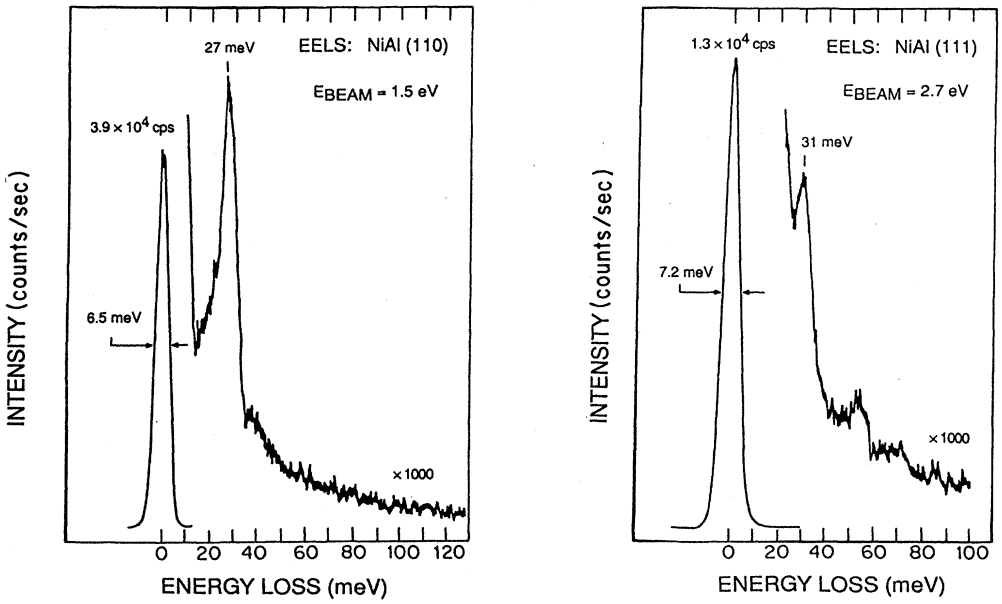

FIG. 4. EELS spectra taken at room temperature showing surface phonon peaks for the (a) (110) and (b) (111) surfaces of NiAl.

NiA(111), Franchy *et al.*[49] identified two peaks observed for the clean surface as dipole-active surface phonon losses; they also saw the C—*M* vibration and the CO stretch on the nominally clean surface. Their frequencies are 28.5 meV (6.90 THz), in fair agreement with our value of 31 meV, and 18 meV (4.35 THz), which is within the bulk LA band along [111] and in fact, close to the peak in the projected bulk LA density of states for this direction. In their EELS spectrum for the nominally clean (111) surface, the structure they mark as the 145-cm^{-1} (18 meV) loss is at best very weak and obscure in the noise of the elastic peak.

B. Calculations

A true surface state is localized in the surface region, and decays exponentially into the bulk. Its frequency must lie in a region where there are no bulk modes of the same symmetry projected onto its surface wave vector. An example is the Rayleigh wave, which splits off below the bulk longitudinal acoustic mode. The surface vibrations we are concerned with are the dipole-active modes at the center of the SBZ, with frequencies in the gap between the acoustic and optic modes. For these surface vibrations, the relevant gap is not the gap in the bulk density of states (see Fig. 3), but rather that between the longitudinal acoustic (LA) and optic (LO) modes propagating along the surface-normal direction in reciprocal space (see Figs. 1 and 2). Put another way, the relevant gap is that in the projected density of states of these bulk LA and LO branches. This gap is of necessity at least as large as the gap in the total bulk DOS, since the latter includes modes of every polarization at all wave vectors throughout the bulk Brillouin zone.

Table VI compares the calculated gaps for the three surfaces with that in the total DOS. The gaps in the projected DOS are all larger by ~50% or more. This point is reinforced by Fig. 5, which shows the projected DOS for the (111) surface.

The (110), (001), and (111) surfaces of NiAl are quite different, as shown in Fig. 6. First, the (110) face is diatomic, with each plane containing a 50-50 mixture of Ni and Al, while the (001) and (111) surfaces are monatomic, with Al layers alternating with layers of Ni. Second, there is a great difference in the atomic density per layer and the interplanar spacing. The (110) surface is the least open, with the largest number of atoms per layer and correspondingly, the largest interplanar spacing. The (111) surface is the most open, having the smallest density per layer and interplanar spacing; the third layer at the (111) surface (whose atoms would lie in the interstices in the top view) is not shadowed by planes 1 and 2, and is actually closer to the surface than the second layer of the (110) face. These structural differences will influence the amount of electronic redistribution that occurs, changes in interatomic force constants, and induced dipole mo-

TABLE VI. Gaps in the bulk phonon density of states and between the LA and LO modes for the three major symmetry directions in NiAl, as calculated with the 3NN force model.

	Gap (THz)	Gap (meV)	Width (THz)
bulk DOS	5.85–7.70	24.2–31.8	1.85
(001)	5.85–8.61	24.2–35.6	2.76
(110)	5.48–8.61	22.7–35.6	3.13
(111)	5.64–8.57	23.3–35.4	2.93

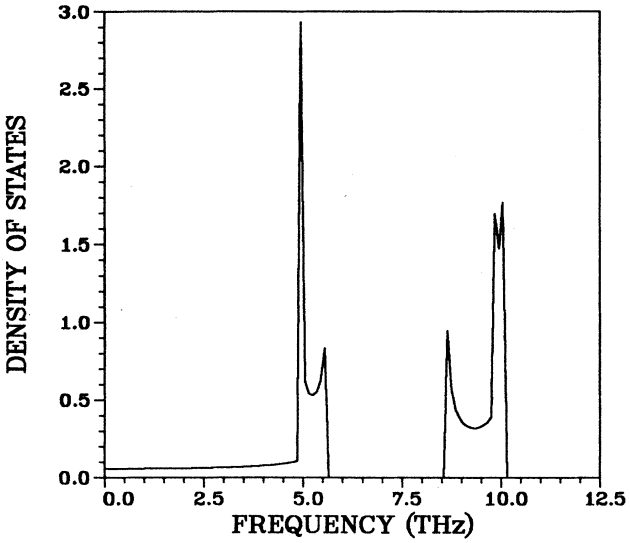

FIG. 5. Projected density of states of the bulk LA and LO modes along [111] in NiAl, from the 3NN model.

ments.

Davis and Noonan have done LEED studies of all three surfaces.[31–34] For (110), they find that the surface is rumpled, with the first-layer Al atoms relaxed outward from second-layer Al atoms by $\Delta d_{12}(\mathrm{Al})=5.2\%$, and the first-second layer Ni-Ni spacing reduced by $\Delta d_{12}(\mathrm{Ni})=-4.6\%$.[32] The total rumple (vertical ripple) between the Al and Ni atoms in the first plane is almost 10%, or 0.20 Å. They also find small second-third layer relaxations of $\Delta d_{23}(\mathrm{Al})=2\%, \Delta d_{23}(\mathrm{Ni})=1\%$. Yalisove and Graham[36] obtained similar results using MEIS; their values for the first-second layer relaxations are $\Delta d_{12}(\mathrm{Al})=5\%$ and $\Delta d_{12}(\mathrm{Ni})=-7\%$. From LEIS Mullins and Overbury[37] concluded that the Al atoms were displaced outward from the Ni atoms by 0.21 ± 0.05 Å, again in good agreement.

Several theoretical calculations have also been done for the relaxation at the (110) surface, all subsequent to the earliest LEED analysis.[31] Kang and Mele[50] and Lee *et al.*[51] each performed electron-density-functional, five-layer slab calculations in which only the atoms in the first layer were allowed to relax (rumple) to equilibrium; other details of their calculations are quite different, but their conclusions are similar except for the size of the outward Al relaxation. Kang and Mele find $\Delta d_{12}(\mathrm{Al})=6.6\%$ and $\Delta d_{12}(\mathrm{Ni})=-6.9\%$, while the values of Lee *et al* are $\Delta d_{12}(\mathrm{Al})=1.5\%$ and $\Delta d_{12}(\mathrm{Ni})=-8.0\%$. The values for the total rumple in the top layer, 13.5% and 9.5%, are in good agreement with the measured values of 9.8–12.0 %. The embedded-atom calculations of Chen *et al.*[52] give much larger values for $\Delta d_{12}(\mathrm{Al})$ and $\Delta d_{12}(\mathrm{Ni})$, predict implausibly large relaxations deep below the surface, and may be disregarded.

The monatomic (001) and (111) surfaces may be terminated by either an Al or a Ni plane. On the basis of *R*-factor analysis of the LEED *I-V* profiles, Davis and Noonan conclude that the (001) face is terminated by Al, and that the first (Al) plane contracts inward while the second (Ni) plane relaxes outward, $\Delta d_{12}=-8.5\%$ and $\Delta d_{23}=4\%$.[34] However, as has been noted, either a $c(3\sqrt{2}\times\sqrt{2})R45°$ or a (1×1) surface structure can be formed depending on the annealing temperature. Also, from LEIS, Mullins and Overbury[37] found that the outermost plane of the NiAl(001):(1×1) surface was a random mixture of 78% Al and 22% Ni, over a second layer that was all Ni. No conclusions about relaxation at the (1×1) surface were drawn in the LEIS study.

For the (111) surface, the LEED analysis[33] of Noonan and Davis led to the somewhat surprising conclusion that

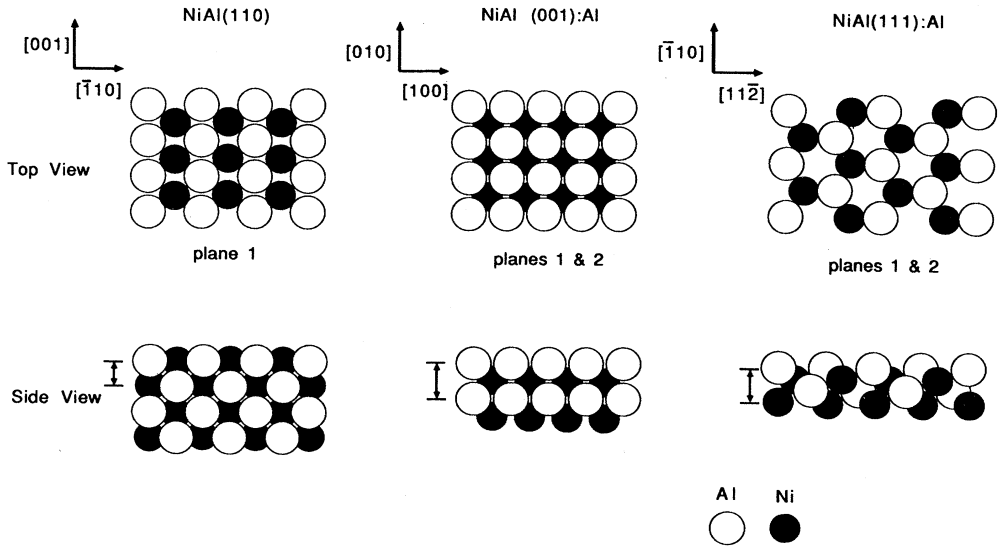

FIG. 6. Ball models for the unrelaxed (110), (001), and (111) faces of NiAl. The arrows at the left of the side views show the range of the interplanar forces in the 3NN model.

NiAl(111) consists of roughly equal areas of both Ni-terminated and Al-terminated domains. For the Al-terminated regions, they find small relaxations of $\Delta d_{12}=-5\%$ and $\Delta d_{23}=5\%$. For the Ni termination, they find much larger relaxations, $\Delta d_{12}=-50\%$ and $\Delta d_{23}=15\%$. Because this is the most open surface, with the smallest interplanar spacing, these interplanar relaxations for the Ni-terminated surface do not represent implausibly large changes in bond lengths; the bond length between a first-layer Ni atom and a second-layer Al atom would decrease by 6%, while that between a Ni atom in the first layer and an Al atom directly below in the fourth plane (see Fig. 6) would decrease by 12%. Using LEIS, Niehus[38] has also concluded that NiAl(111) is an approximately 50-50 mixture of Ni- and Al-terminated domains.

One of the purposes of the present work was to try to demonstrate that in some cases surface phonon spectroscopy and calculations could determine the termination at surfaces like NiAl(111) and (001). Our results will prove to be equivocal. For (111), where an EELS vibrational-loss peak is observed, the calculations show at least three possible surface modes, one for the Ni and two for the Al termination, and with no force-constant changes these are spaced fairly closely in frequency. For (001), the calculated surface mode frequencies for the two terminations appear likely to be rather different, but no surface dipole-active gap mode has been seen as yet.

The calculations we have done are slab calculations at the SBZ center, based on the 3NN force model fitted to the bulk phonon data. All results quoted are for very thick slabs of 50–100 layers for (110) and 101-201 layers for (001) and (111). Calculations assuming no force-constant changes indicate that NiAl is likely to have a rich variety of surface states. There are gap modes for each of the three surfaces, not only for the dipole-active vibrations normal to the surface, but also for vibrations parallel to the surface. The only exception is (001), for which there is no gap mode for vibrations parallel to the surface.

To fit the calculated frequencies to the measured loss peaks, force-constant changes must be included in the theoretical model. If only one gap-mode frequency has been measured for a particular face, it is clearly not possible to determine all force-constant changes in the surface region. We have therefore resorted to some reasonable simplifying assumptions. By far the largest pairwise interactions in the bulk are the 1NN Ni-Al and the 2NN Al-Al interactions (see Table II). Suppose these interactions result from central pair potentials $v(r)$, where r is the interatomic distance. The force-constant matrix between the pair of ions then is

$$\Phi_{ij}(r)=[A(r)-B(r)]r_i r_j/r^2+B(r)\delta_{ij}\ , \tag{3}$$

$$A(r)=v''(r)\ , \tag{4}$$

$$B(r)=v'(r)/r\ . \tag{5}$$

$A(r)$ is the radial force constant given in Tables I–III and $B(r)$ is the tangential force constant, which for near neighbors is generally much smaller than A.

For pairwise force-constant matrices where the crystal symmetry allows only two independent parameters, as for the 1NN and 2NN forces in NiAl, there is a one-to-one relationship between the two elements of the force-constant matrices and the radial and tangential force constants. Table III gives the relation between A and the force-constant matrix elements for (111) and (200) neighbors. For our 3NN model, the radial force constants for the 1NN Ni-Al and 2NN Al-Al coupling are A(Ni-Al)=31420 dyn/cm and A(Al-Al)=18 380 dyn/cm, respectively.

We denote the interplanar force constant between b-type atoms in layer L and b' atoms in layer L' as $K(L,b;L',b')$; these interplanar force constants are linear combinations of interatomic force constants for which the bulk values are given in Table II. Force-constant changes $dK(L,b;L',b')$ will be given as fractions of the bulk values. To fit the experimental frequencies, we will vary only those interplanar force constants that include the 1NN Ni-Al and 2NN Al-Al radial interactions, and that involve at least one atom in the outermost layer. Even with this simplification, unambiguous values for force-constant changes cannot be assigned where there is one experimental frequency and more than one large interplanar force constant. However, the displacements are generally similar for different force-constant changes that produce the same frequency, and it is possible to identify the force constants that are most important for the mode in question.

An example is provided in Fig. 7. As already dis-

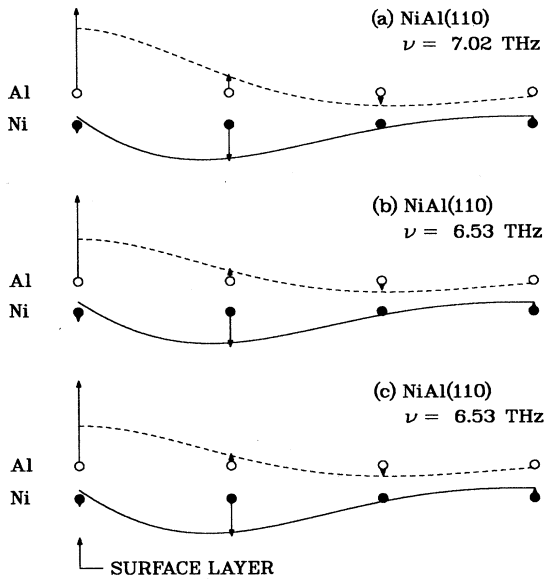

FIG. 7. Calculated surface-normal displacement amplitudes of atoms in the first four planes for the gap mode on NiAl(110) for (a) no force-constant changes, (b) $dK(1,\mathrm{Al};2,\mathrm{Ni})=dK(1,\mathrm{Al};2,\mathrm{Al})=-0.211$, and (c) $dK(1,\mathrm{Al};2,\mathrm{Ni})=-dK(1,\mathrm{Ni};2,\mathrm{Al})=-0.173$. The outermost layer is at the left, and the displacements are shown as vertical lines (rather than horizontal, along the surface-normal direction) for display purposes. Only relative values of the displacements are meaningful. The force-constant changes dK are fractions of the bulk values, e.g., $K(1,\mathrm{Al};2,\mathrm{Ni})=[1+dK(1,\mathrm{Al};2,\mathrm{Ni})]K_{\mathrm{bulk}}(L,\mathrm{Al};L+1,\mathrm{Ni})$.

cussed, other experimental and theoretical analyses indicate that the (110) surface is rumpled, with the Al atoms in the first plane relaxing outward and the Ni atoms in plane 1 relaxing inward, both by about 5% of the bulk interlayer spacing. We might therefore expect the forces between Al atoms in plane 1 and atoms in deeper layers to decrease, and those between surface layer Ni atoms and neighbors in other layers to increase. As the figure shows, modest force-constant changes that follow the expected pattern are precisely what is required to move the calculated frequency down from the truncated bulk value of 7.02 THz to the measured 6.53 THz. The solid curves in Fig. 7 are simple functions that we will discuss presently.

The displacement patterns in Fig. 7 are quite different from those found by Kang and Mele[50] from their electronic calculations of the surface structure. Kang and Mele are essentially doing what are called frozen-phonon calculations, and by assumption, they allow only atoms in the first layer to move, either statically or vibrationally. Thus, although their calculated frequency agrees exactly with our measured value, they find large displacements of the first-layer Ni atoms [$u(1,\mathrm{Ni}) = -0.4u(1,\mathrm{Al})$], having constrained all motion in deeper layers to be zero. This illustrates a major deficiency of frozen-phonon calculations at surfaces. By making limiting assumptions, such calculations define the displacement patterns (within limits) and then use these to calculate the frequencies, when the actual displacements may extend much deeper into the crystal. This vibrational response deeper in the crystal may in turn affect the frequency.

A much more desirable method of using electronic calculations to study surface vibrations is illustrated by the work of Ho and Bohnen[53] on Al(110). The electronic calculations are used first to determine the relaxed equilibrium surface structure, and second, to find the intraplanar and interplanar force-constant changes to some reasonable depth into the crystal. The latter are then incorporated into thick slab calculations that make no assumptions about the displacements, in the realization that the displacements for the surface vibrations may extend deeper into the crystal than do the static relaxation or the changes in the forces.

A much more desirable method of using electronic calculations to study surface vibrations is illustrated by the work of Ho and Bohnen[53] on Al(110). The electronic calculations are used first to determine the relaxed equilibrium surface structure, and second, to find the intraplanar and interplanar force-constant changes to some reasonable depth into the crystal. The latter are then incorporated into thick slab calculations that make no assumptions about the displacements, in the realization that the displacements for the surface vibrations may extend deeper into the crystal than do the static relaxation or the changes in the forces.

The solid curves in Fig. 7 represent fits to the asymptotic decay of the surface vibrations into the bulk. The functional form fitted is an exponential x cosine,

$$u(L,b) = A(b)\exp[-\alpha z(L,b)]\cos[q_z z(L,b)+\phi(b)] , \quad (6)$$

where $u(L,b)$ is the displacement of atom b in layer L and $z(L,b)$ is the depth of this atom in the crystal. As shown in Fig. 7, the displacements in planes 2 and deeper are given rather well by Eq. (6), with parameters we will discuss presently, while the displacements in layer 1 are not. Without going into great detail, we use the following two-step procedure to determine the parameters in Eq. (6): (1) estimate a trial value $\tilde{\alpha}$ for the exponential decay, and (2) find final values for α, A, q_z, and ϕ by a least-squares fit to $\exp[+\tilde{\alpha}z(L,b)]u_{\mathrm{slab}}(L,b)$, where $u_{\mathrm{slab}}(L,b)$ are the displacements from the slab calculations. In doing this, we take note of two additional factors. First, the actual displacement pattern is a superposition of a surface disturbance in the first few layers and the asymptotic decay, and it is only the latter that we model according to Eq. (6). Second, slab calculations impose symmetries (evenness or oddness) that constrain the displacements at the slab center. We therefore apply other numerical criteria that may eliminate from the fitting procedure some layers from the first on down into the crystal and some from the middle of the slab up. Pictures like Fig. 7 do not do justice to how well Eq. (6) describes the asymptotic behavior because they include the first one or several layers where Eq. (6) does not apply, and because the exponential decay makes the displacements small where it does.

The oscillatory behavior in the asymptotic decay, that is, the wave vector q_z in the cosine in Eq. (6), is related to, or in some sense determined by, the nature of the bulk longitudinal modes. Figure 8 shows the calculated dispersion curves for the longitudinal branches only, and the measured surface phonon frequencies are drawn as horizontal lines in the gap. Along the [110] and [111] directions, the dashed lines show what the dispersion would have looked like if the modes had not hybridized to form a gap. No hybridizationlike behavior is evident for the gap along [001].

To reinforce this point, we plot in Fig. 9 the longitudinal dispersion curves for CuZn, in which the constituents

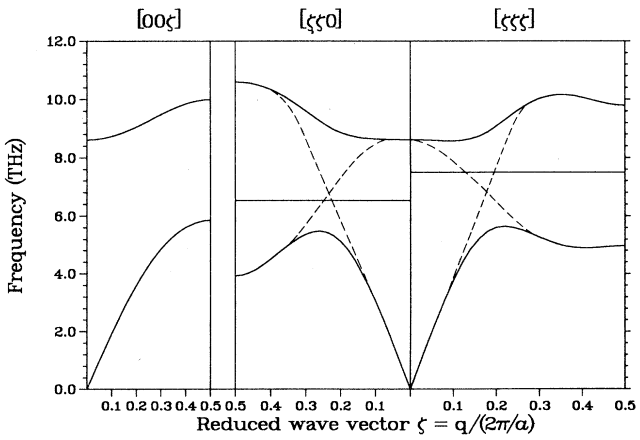

FIG. 8. 3NN bulk longitudinal dispersion curves for NiAl. The horizontal lines show the measured EELS loss frequencies, and the dashed lines the branches as they might have been before hybridization.

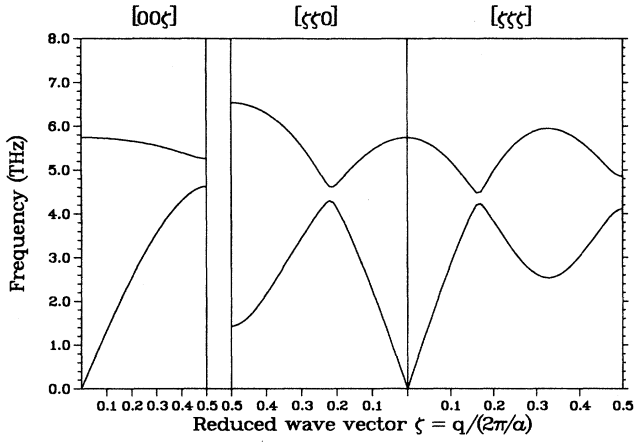

FIG. 9. Calculated longitudinal phonon dispersion curves for CuZn (β-brass).

have almost equal masses. The force constants are taken from Gilat and Dolling.[11] The LA and LO modes almost cross, but instead must hybridize, at $\zeta \sim 0.22$ and 0.17 along [110] and [111], respectively.

The point is that the oscillations in the surface gap-mode displacements are localized in q_z for the (110) and (111) surfaces by this hybridizationlike behavior. This is illustrated in Table VII for the (110) face, where the parameters in Eq. (6) are given as the frequency of the gap mode is moved from just above the LA mode to about 1 THz below the LO mode; recall from Table VI that the gap for this surface is 5.48–8.61 THz. Figure 10 shows the displacements for the lowest, measured, and highest frequencies in Table VII.

Just above the maximum frequency of the LA mode, the exponential decay parameter α is small, and the amplitude for the Al atoms is negligible (except for the first layer), so we have a predominantly Ni mode that extends deep into the crystal as shown in the top panel of Fig. 10. As we move the frequency up beyond midgap, α increases and the exponential decays more rapidly, while the amplitudes $A(b)$ change to increase the relative strength for Al and the phases $\phi(b)$ vary by small amounts. What is striking, however, is that q_z stays pinned near the hybridization wave vector $q_z \sim 0.33 \times (2\pi/a)$ for this direction (see Fig. 8, and note that a factor of $\sqrt{2}$ is included in q_z) as the frequency is varied over about two-thirds of the gap.

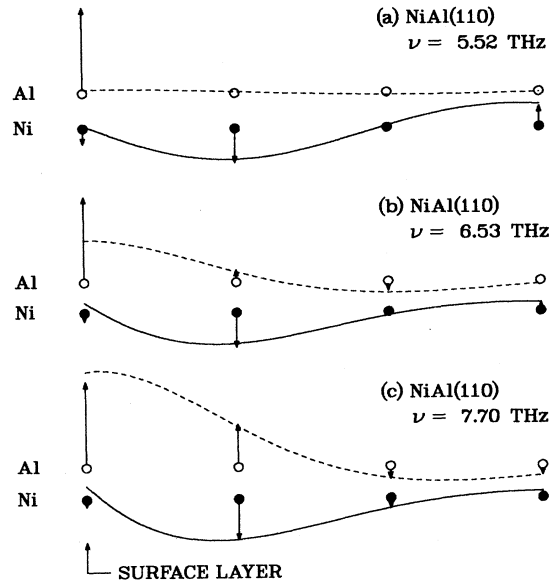

FIG. 10. Calculated surface-normal displacement amplitudes for the gap mode with the lowest, measured, and highest frequencies in Table VII.

For the (111) surface, as already discussed, LEED (Ref. 33) and LEIS (Ref. 38) indicate that there is an approximately 50-50 mixture of Al- and Ni-terminated domains. Our calculations show that gap modes should occur for either termination. They are invariably localized on Al planes. In the absence of force-constant changes, the Al-terminated surface has two modes with frequencies of 6.78 and 8.10 THz, with the maximum displacement at planes 1 and 3, respectively. For the Ni termination, there is one surface state in the gap with a frequency of 7.31 THz and localized on plane 2. For the sake of brevity, we will refer to these modes by the index of the Al plane with the largest displacement amplitude, so the two states at the Al-terminated surface are modes 1 and 3, while the one for the Ni termination is mode 2. Note that the total spread in frequency for the three modes is 1.32 THz (5.5 meV), and that modes 1 and 2 are separated by only 0.53 THz (2.2 meV).

By changing the force constants at the surface, each of the three calculated modes can be shifted to the measured frequency of 7.50 THz. This is illustrated in Fig. 11. For mode 1, the largest force constants must be increased by

TABLE VII. Parameters for the exponental x cosine fit to the decay of the displacements of the surface mode at NiAl(110). For comparison, the hybridization wave vector along the [110] direction is $q_z/(2\pi/a) \sim 0.33$. All results are for force-constant changes $dK(1,\mathrm{Al};2,\mathrm{Ni}) = -dK(1,\mathrm{Ni};2,\mathrm{Al})$. An asterisk marks the entry that fits the measured frequency.

dK	ν	α/d	$q_z/(2\pi/a)$	A(Al)	ϕ(Al)	A(Ni)	ϕ(Ni)
−0.600	5.52	0.14	0.37	0.05	−2.10	0.48	−0.14
−0.400	6.05	0.49	0.36	0.43	−2.06	0.92	−0.16
−0.211*	6.53	0.64	0.35	1.02	−1.95	1.34	−0.14
0.000	7.02	0.74	0.33	1.75	−1.91	1.77	−0.03
0.200	7.44	0.79	0.32	2.35	−1.94	2.15	0.05
0.350	7.70	0.81	0.31	3.60	−2.03	2.51	0.05

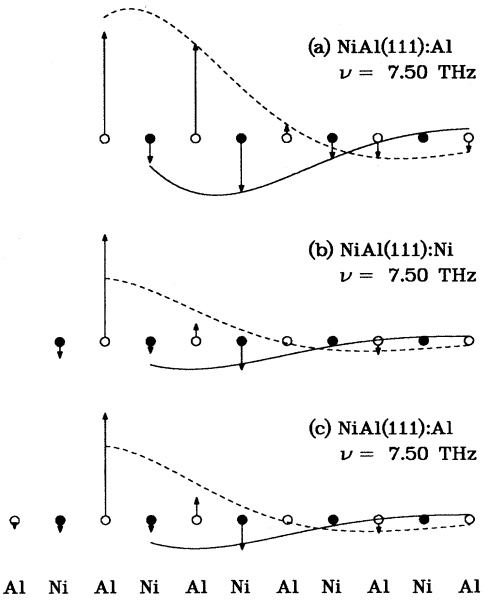

FIG. 11. Calculated surface-normal displacement amplitudes for modes 1–3 on NiAl(111), with force-constant changes to fit the measured frequency: (a) $dK(1,\mathrm{Al};2,\mathrm{Ni}) = dK(1,\mathrm{Al};3,\mathrm{Al}) = dK(1,\mathrm{Al};4,\mathrm{Ni}) = 0.402$, (b) $dK(1,\mathrm{Ni};2,\mathrm{Al}) = dK(1,\mathrm{Ni};4,\mathrm{Al}) = 0.311$, and (c) $dK(1,\mathrm{Al};2,\mathrm{Ni}) = dK(1,\mathrm{Al};3,\mathrm{Al}) = dK(1,\mathrm{Al};4,\mathrm{Ni}) = -0.724$.

about 40%, and the interlayer force constant that has the greatest effect is the first-layer–fourth-layer coupling $K(1,\mathrm{Al};4,\mathrm{Ni})$. This is easily understood from the side view of the (111) surface in Fig. 6. Directly below an Al atom in plane 1 is a first-neighbor Ni atom in plane 4. This 1NN, plane-1—plane-4 bond will change in length by the full amount of the interplanar relaxation at the surface, while the first-layer–second-layer and first-layer–third-layer bond-length changes will be reduced by the cosines of the angles between the bonds and the surface normal. With the force-constant changes for mode 1 in Fig. 11, a second gap mode is predicted at 8.52 THz, just below the LO band, with its maximum displacement at plane 7 and extending deep into the crystal from there; it is unlikely that a mode localized so deep in the crystal would generate a dipole moment that would make it observable.

For mode 2, i.e., for the Ni-terminated surface, an increase of about 30% in the largest forces is required, particularly in $K(1,\mathrm{Ni};2,\mathrm{Al})$ to fit the measured frequency. The plane-1–plane-4 interaction is not as effective in this case because it does not involve either plane 2, which has the largest displacement, or plane 5, which has the second largest. To shift the frequency of mode 3 to the observed value requires a very considerable reduction of $\sim 70\%$ in the force constants, and, again reflecting the displacement pattern for the mode, the most important interplanar force constant appears to be $K(1,\mathrm{Al};3,\mathrm{Al})$. Mode 1 is driven down into the acoustic band by this large reduction in the forces.

The question is which of modes 1–3 is responsible for the EELS loss peak. As shown in Fig. 4, the intensity of the peak for the (111) face is roughly 4 times smaller than that for (110). To get a very crude estimate of the relative magnitude of the dynamic dipole moments for the three surfaces, we do the following: (1) assume the effective charges of Ni and Al are the same and independent of the surface, (2) neglect motion of layers below the first, (3) calculate the dynamic dipole from the rms displacement (at 300 K) divided by the area per atom, and (4) for (110), where Al and Ni vibrate out of phase, add the values for the two atoms. The results, scaled to the (110) surface, are (110)−1, (001):Al−0.52, (111):Al−0.25, and (111):Ni−0.10. These crude estimates are that the least open face will have the largest dipole moment and the most open the smallest, down by a factor of 4–10, which is not inconsistent with the strengths of the observed loss peaks for (110) and (111).

The displacements in Fig. 11 suggest that the dynamic dipole moments for the (111) surface produced by the three calculated gap modes would be ordered $1>2>3$. Mode 3 would appear to have a very small dipole moment, since planes 1 and 2 are essentially stationary, and following the arguments of Rahman *et al.*[54] the motion of plane 3 would be screened by approximately $\exp\{-k_F[z(3)-z(1)]\}$. Furthermore, an implausibly large reduction in the forces is needed to shift it to the measured frequency, particularly since the LEED analysis for the Al termination gives only a 5% contraction and expansion in d_{12} and d_{23}, respectively (and no change in d_{13}). We therefore rule out mode 3 as the source of the EELS loss peak. Although this mode will probably be present at a higher frequency for the Al-terminated surface, it is not likely to be observed by EELS.

This leaves modes 1 and 2 as possible sources for the EELS peak, and we find little reason to choose between them, particularly since the two modes are so close in frequency for the truncated bulk crystal. The very crude estimates of relative dynamic dipole moments that we have done do not allow us to choose, since they give values within a factor of 3 for the two terminations, and these estimates rest on assumptions that are very questionable for a surface for which the first three layers are not shadowed by layers above. Mode 1 begins at a lower frequency for the truncated bulk, is more easily shifted by force-constant changes, and, according to LEED,[33] the Al-terminated domains undergo small relaxations ($\Delta d_{12} = -5\%$). Mode 2 is harder to move, but the interplanar spacings apparently change by rather large amounts ($\Delta d_{12} = -50\%$). We might argue that since the measured relaxations are much smaller for the Al-terminated than the Ni-terminated domains, and yet our calculations require larger force-constant changes for the former than for the latter, that it is mode 2, i.e., the Ni termination, that we have observed. What does seem to be clear from the calculations is that if the surface really is a mixture of Al and Ni terminations, then there will be at least two surface gap modes.

We turn our attention now to the asymptotic behavior of the displacement patterns for the (111) surface; that is, to the parameters in the exponential x cosine function of Eq. (6). These are given for a variety of force-constant

changes for the two terminations in Table VIII. The exponential decays more slowly into the bulk as the frequency approaches the top of the LA band or the bottom of the LO band, but α always has the same value for different force-constant changes and termination combinations that reproduce the measured frequency. The amplitudes $A(b)$ and phases $\phi(b)$ appear to vary in a reasonable way as particular force-constant combinations are varied. Most important, as for (110), the wave vector for the oscillations in z remains close to the hybridization wave vector $q_z \sim 0.31(2\pi/a)$.

Figure 12 shows displacement patterns for mode 1 in the absence of force-constant changes and for three different force-constant changes that fit the measured frequency. The displacements are similar in all four panels and extend rather deep (about seven to nine layers) into the bulk. This shows that the displacement patterns do not depend a great deal on the particular set of force-constant changes used to obtain the observed frequency.

For the (001) surface of NiAl, we have been unable to observe any surface vibrational losses by EELS, perhaps due to the experimental difficulties described previously. However, the slab calculations do predict that a dipole-active gap mode will occur, and we can estimate its frequency from simple arguments.

According to the LEED work,[34] the (001) surface is terminated by an Al plane and the first interplanar spacing contracts by 8.5% while the second expands by 4%. For this termination with no force-constant changes, the calculations predict a surface state with a frequency of 7.08 THz (29.3 meV), just below the middle of the gap of 5.85–8.61 THz. If the surface were Ni-terminated, the frequency of the calculated gap mode in the absence of force-constant changes would be 8.47 THz (35.0 meV), substantially higher. NiAl(001) is therefore an example of a surface for which measuring the frequency of the dipole-active surface vibration might be helpful in establishing the termination.

For the (001) surface, the bond-length changes from LEED are -0.04 and -0.03 Å between first-layer Al atoms and second-layer Ni and third-layer Al atoms. For the diatomic (110) surface, the relaxations determined by LEED (Ref. 32) correspond to bond-length changes of $+0.05$ and $+0.07$ Å between first-layer Al atoms and second-layer Al and Ni atoms. For (110), a decrease of about 20% in the corresponding interplanar force constants (see the caption for Fig. 7) brought the calculated frequency into agreement with the experimental value. If

TABLE VIII. Parameters for the exponential x cosine fit to the decay of the displacements of the surface modes at NiAl(111). T denotes the type of layer that terminates the crystal and L the index of the layer that has the maximum displacement in the surface vibration. For comparison, the hybridization wave vector along the [111] direction is $q_z/(2\pi/a) \sim 0.31$. Asterisks mark the entries that fit the measured frequency.

T	L	dK	ν	α/d	$q_z/(2\pi/a)$	A(Al)	ϕ(Al)	A(Ni)	ϕ(Ni)
			A: $dK(1,\text{Al};2,\text{Ni})=dK(1,\text{Al};3,\text{Al})=dK(1,\text{Al};4,\text{Ni})=0.402$						
			B: $dK(1,\text{Ni};2,\text{Al})=dK(1,\text{Ni};4,\text{Al})=0.311$						
			C: $dK(1,\text{Al};2,\text{Ni})=dK(1,\text{Al};3,\text{Al})=dK(1,\text{Al};4,\text{Ni})=-0.724$						
Al*	1	A	7.50	0.31	0.29	2.28	−1.35	1.79	0.78
Ni*	2	B	7.50	0.31	0.29	1.21	−1.50	1.00	0.56
Al*	3	C	7.50	0.31	0.29	1.95	−2.04	1.45	−0.02
			A: $dK(1,\text{Al};2,\text{Ni})=dK(1,\text{Al};3,\text{Al})=dK(1,\text{Al};4,\text{Ni})=0.402$						
			D: $dK(1,\text{Al};4,\text{Ni})=0.513$						
			E: $dk(1,\text{Al};2,\text{Ni})=1.540$						
Al*	1	A	7.50	0.31	0.29	2.28	−1.35	1.79	0.78
Al*	1	D	7.50	0.31	0.29	2.30	−1.30	1.84	0.84
Al*	1	E	7.50	0.31	0.29	1.85	−1.41	1.37	0.68
			$dK(1,\text{Al};2,\text{Ni})=dK(1,\text{Al};3,\text{Al})=dK(1,\text{Al};4,\text{Ni})$						
Al	1	−0.400	5.69	0.07	0.37	0.09	−1.86	0.60	0.45
Al	1	−0.200	6.26	0.23	0.35	0.49	−1.41	0.89	0.54
Al	1	0.000	6.78	0.28	0.33	0.97	−1.37	1.19	0.64
Al	1	0.200	7.19	0.30	0.31	1.57	−1.36	1.48	0.70
Al*	1	0.402	7.50	0.31	0.29	2.28	−1.35	1.79	0.78
Al	3	0.500	7.62	0.31	0.29	2.56	−1.33	1.85	0.82
Al	3	0.900	7.99	0.29	0.26	2.43	−1.22	1.39	1.06
			$dK(1,\text{Ni};2,\text{Al})=dK(1,\text{Ni};4,\text{Al})$						
Ni	2	−0.600	6.99	0.29	0.32	1.37	−1.82	1.51	0.19
Ni	2	0.000	7.31	0.31	0.30	1.43	−1.56	1.18	0.40
Ni*	2	0.311	7.50	0.31	0.29	1.21	−1.50	1.00	0.56
Ni	2	0.600	7.68	0.31	0.28	1.30	−1.30	0.85	0.75

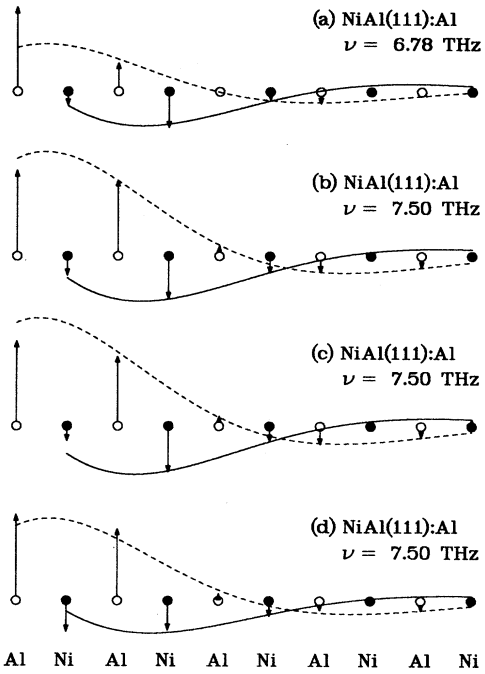

FIG. 12. Surface-normal displacement amplitudes for mode 1 for NiAl(111):Al with (a) no force-constant changes, (b) $dK(1,\mathrm{Al};2,\mathrm{Ni})=dK(1,\mathrm{Al};3,\mathrm{Al})=dK(1,\mathrm{Al};4,\mathrm{Ni})=0.402$, (c) $dk(1,\mathrm{Al};4,\mathrm{Ni})=0.513$, and (d) $dk(1,\mathrm{Al};2,\mathrm{Ni})=1.54$.

we scale the force-constant changes for (001) from those for (110) by the ratio of the changes in the bond lengths, this is, by a factor of $\sim-\frac{1}{2}$, we might expect $K(1,\mathrm{Al};2\mathrm{Ni})$ and $K(1,\mathrm{Al};3,\mathrm{Al})$ to increase by about 10%. With such an increase, the calculated frequency for NiAl(001) is 7.4 THz (31 meV).

Because there is no hybridization of the bulk LA and LO modes along the [001] direction, the decay of the gap vibrations for the (001) surface is qualitatively different than for (110) and (111). Instead of the exponential x cosine behavior seen for the latter two faces, what occurs is either simple exponential decay or an oscillatory exponential pattern. For the Al termination, odd (Al) planes have indexes $L=2m-1$, and even (Ni) planes $L=2m$, $m=1,2,\ldots$. Modes below a crossover frequency ν_c, here ~ 7.5 THz, decay asymptotically as oscillatory exponentials,

$$u(L,b)=(-1)^m A(b)\exp[-\alpha z(L)] \ . \tag{7a}$$

The displacements oscillate in sign every like-atom plane. Modes above this frequency decay as simple exponentials,

$$u(L,b)=A(b)\exp[-\alpha z(L)] \ . \tag{7b}$$

Near the crossover frequency, these decay patterns obtain only very deep in the crystal. An alternative way to characterize this behavior is to say that below ν_c the mode oscillates with the zone-boundary wave vector π/a, while above ν_c it is at the zone center.

Figure 13 shows the oscillatory and simple exponential

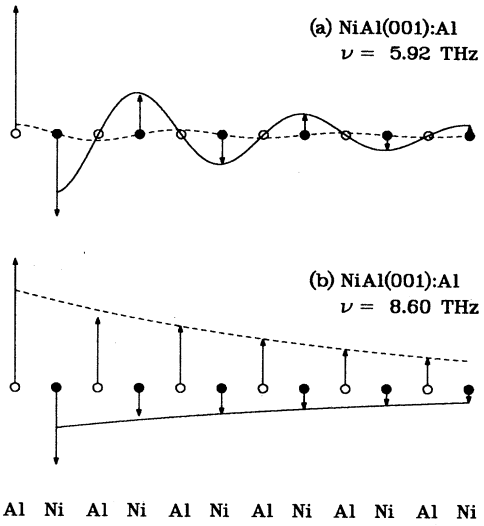

FIG. 13. Surface-normal displacement amplitudes for NiAl(001):Al with $dK(1,\mathrm{Al};2,\mathrm{Ni})=dK(1,\mathrm{Al};3,\mathrm{Al})=(a)$ -0.350 and (b) 0.600.

decay for NiAl(001) for force-constant changes that put the surface mode just above the top of the bulk LA band (5.85 THz) and just below the LO-band minimum (8.61 THz). Table IX gives the changes in parameters and type of behavior as the mode is shifted across the gap. The surface vibration decays slowly in the proximity of either the bulk LA or LO mode, as shown in Fig. 13, and much more rapidly in the middle of the gap.

Stroscio *et al.* have observed resonances in what they refer to as "pseudo band gaps" in the bulk LA density of states for the (110) surfaces of Cu and Ni,[22] and later for Fe(111).[23] For these surfaces, the dispersion of the bulk LA modes along the [110] and [111] directions, respectively, is similar to that for both directions in NiAl (see Figs. 1, 2, and 8). A consequence of this nonmonotonic dispersion is that most of the weight in the LA projected density of states lies in a relatively narrow structure of peaks near the top of the spectrum, such as that shown in Fig. 5 for the LA mode along [111] in NiAl. The reduction in coordination at the surface results in a surface

TABLE IX. Parameters for the simple or oscillatory exponential fit to the displacements of the surface modes at NiAl(001):Al. All results are for force-constant changes $dK(1,\mathrm{Al};2,\mathrm{Ni})=dK(1,\mathrm{Al};3,\mathrm{Al})$, with the maximum displacement on plane 1. In the column "Type," *O* denotes oscillatory and *S* simple exponential behavior.

dK	ν	Type	α/d	A(Al)	A(Ni)
−0.350	5.92	*O*	0.17	0.09	−0.64
−0.200	6.42	*O*	0.49	0.33	−0.93
0.000	7.08	*O*	0.72	0.61	−1.18
0.100	7.38	*O*	0.81	0.75	−1.31
0.200	7.67	*S*	0.82	1.97	−1.43
0.315	7.98	*S*	0.69	1.82	−1.41
0.500	8.42	*S*	0.39	1.34	−0.69
0.600	8.60	*S*	0.11	0.85	−0.39

density of states (DOS) with a large peak below the strong structure in the bulk projected DOS, that is, in a region of low bulk spectral density or a "pseudo band gap."

One reason we have performed calculations for very thick slabs of 100 layers for the (110) surface and 201 layers for (001) and (111) is to have enough modes to do a rough calculation of the densities of states for the various layers. We do this by sorting the frequencies into histogram bins and weighting with the square of the eigenvector for the layer. Surface resonances such as those discussed by Stroscio *et al.* do seem to occur for both the (110) and (111) surfaces, just below the strong structure in the bulk LA projected DOS. For the (110) face, with force-constant changes that fit the measured gap-mode frequency, there appears to be a resonance in the range 3.4–3.8 THz, pseudolocalized on the Ni atoms in planes 1 and 2. For Al-terminated (111), there is a resonance at 4.4–4.8 THz (18–20 meV) on Ni plane 2, while for the Ni termination the resonance is at 3.8–4.2 THz (16–18 meV) on Ni plane 1. For the (001) surface, the calculations do not predict any resonances, and none is expected because the LA dispersion along [001] in the bulk is monotonic.

We have not observed these resonances in our EELS spectra, Franchy *et al.*,[49] however, do identify a weak peak at 4.35 THz (18 meV) in their EELS measurement on clean NiAl(111) as a surface vibrational loss. This is consistent with our calculated results for either termination.

IV. CONCLUSIONS

The neutron-scattering experiments and Born–von Kármán analysis show that the bulk dispersion curves of NiAl can be described very well with a 4NN force model, except for the Kohn-like anomaly in the TA_1 mode along the [110] direction. A 3NN model gives an adequate fit to the data for the purpose of the surface phonon calculations. Dipole-active surface vibrations have been observed by EELS for the (110) and (111) faces, but not for (001).

We have performed extensive slab calculations based on the 3NN force model. All calculated surface states have their maximum displacements on Al planes or atoms. To shift the calculated gap-mode frequencies to the measured values, one must change the largest interplanar force constants in ways that are intuitively consistent with the experimentally determined relaxations. The force constants that are most effective in shifting the frequency for a given surface are dictated by the bond lengths affected most by relaxation and by the displacement pattern. The displacement amplitudes for the surface states appear to be relatively insensitive to the particular set of force-constant changes used to match the measured frequency. We predict a surface gap mode for the (001) surface at a frequency estimated to be $\nu=7.4$ THz (31 meV).

In bulk NiAl along the [110] and [111] directions in reciprocal space, the LA and LO modes exhibit hybridizationlike behavior. This bulk property effectively localizes the surface gap modes in the wave vector q_z normal to the surface; the gap modes decay exponentially into the bulk with oscillations pinned near the hybridization wave vector. For (001), no hybridization occurs in the bulk, and the gap modes behave as if located at the zone boundary or the zone center.

The dispersion of the LA mode along the [110] and [111] directions in NiAl is nonmonotonic, similar to the LA mode along [110] in fcc metals and along [111] in bcc metals. The slab calculations predict resonances for NiAl in the surface Ni densities of states like those observed for Cu(110), Ni(110), and Fe(111).

Finally, we return to a point mentioned briefly in Sec. III. In the absence of force-constant changes, and with the exception of vibrations parallel to the surface for (001), the slab calculations predict gap modes for all three surfaces and all terminations for every polarization. NiAl would therefore appear to be an excellent candidate for the study of surface vibrations throughout the SBZ's of the various faces, and of the changes in interatomic forces at the surfaces of an ordered metal alloy.

ACKNOWLEDGMENTS

We would like to thank Gary Ownby for invaluable help with sample preparation and characterization. We have benefited from useful conversations with H. L. Davis, A. P. Baddorf, J. F. Wendelken, and E. J. Mele. This work was sponsored by Oak Ridge National Laboratory under U.S. Department of Energy Contract No. DE-AC05-84OR21400 with Martin Marietta Energy Systems, Inc. One of us (S.-C.L.) would like to thank the Oak Ridge National Laboratory for financial support.

*Present address: National Synchrotron Light Source, Brookhaven National Laboratory, P.O. Box 709, Upton NY 11973-6000.

†Present address: IBM Corporation, Essex Junction, VT 05452.

[1]B. N. Brockhouse, K. R. Rao, and A. D. B. Woods, Phys. Rev. Lett. **7**, 93 (1961).

[2]R. J. Birgeneau, J. Cordes, G. Dolling, and A. D. B. Woods, Phys. Rev. **136**, A1359 (1964).

[3]G. Gilat and R. M. Nicklow, Phys. Rev. **143**, 487 (1966).

[4]R. Stedman and G. Nilsson, Phys. Rev. **145**, 492 (1966).

[5]V. J. Minkiewicz, G. Shirane, and R. Nathans, Phys. Rev. **162**, 528 (1967).

[6]C. van Dijk, Reactor Centrum Nederland (Petten, The Netherlands) Report No. RCN-129, 1970 (unpublished).

[7]S. K. Sinha, Phys. Rev. **143**, 422 (1966).

[8]E. C. Svensson, B. N. Brockhouse, and J. M. Rowe, Phys. Rev. **155**, 619 (1967).

[9]R. M. Nicklow, G. Gilat, H. G. Smith, L. J. Raubenheimer, and M. K. Wilkinson, Phys. Rev. **164**, 922 (1967).

[10]G. Borgonovi, G. Caglioti, and J. J. Antal, Phys. Rev. **132**, 683 (1963).

[11]G. Gilat and G. Dolling, Phys. Rev. **138**, A1053 (1965).

[12]H. G. Smith and W. Gläser, Phys. Rev. Lett. **25**, 1611 (1970); in *Proceedings of the International Conference on Phonons,* Rennes, 1971, edited by M. Nusimovici (Flammarion Sciences, Paris, 1971).
[13]C. Stassis, F. X. Kayser, C.-K. Loong, and D. Arch, Phys. Rev. B **24**, 3048 (1981).
[14]S. M. Shapiro, J. Z. Larese, Y. Noda, S. C. Moss, and L. E. Tanner, Phys. Rev. Lett. **57**, 3199 (1986), and references therein; S. M. Shapiro, B. X. Yang, G. Shirane, Y. Noda, and L. E. Tanner, *ibid.* **62**, 1298 (1989).
[15]G. Brusdeylins, R. B. Doak, and J. P. Toennies, Phys. Rev. Lett. **46**, 437 (1981).
[16]H.-J. Ernst, E. Hulpke, and J. P. Toennies, Phys. Rev. Lett. **58**, 1941 (1987).
[17]For a review, see H. Ibach and D. L. Mills, *Electron Energy Loss Spectroscopy and Surface Vibrations* (Academic, New York, 1982).
[18]H. Ibach and D. Bruchmann, Phys. Rev. Lett. **41**, 958 (1978).
[19]S. Lehwald, J. M. Szeftel, H. Ibach, T. S. Rahman, and D. L. Mills, Phys. Rev. Lett. **50**, 518 (1983).
[20]M. Wuttig, R. Franchy, and H. Ibach, Solid State Commun. **57**, 445 (1986).
[21]M. H. Mohamed, L. L. Kesmodel, B. M. Hall, and D. L. Mills, Phys. Rev. B **37**, 2763 (1988).
[22]J. A. Stroscio, M. Persson, S. R. Bare, and W. Ho, Phys. Rev. Lett. **54**, 1428 (1985).
[23]J. A. Stroscio, M. Persson, C. E. Bartosch, and W. Ho, Phys. Rev. B **33**, 2879 (1986).
[24]C. Oshima, R. Souda, M. Aono, S. Otani, and Y. Ishizawa, Phys. Rev. B **30**, 5361 (1984); Solid State Commun. **57**, 283 (1986); Phys. Rev. Lett. **56**, 240 (1986).
[25]C. Oshima, Phys. Rev. B **34**, 2949 (1986).
[26]M. Wuttig, C. Oshima, T. Aizawa, R. Souda, S. Otani, and Y. Ishizawa, Surf. Sci. **192**, 573 (1987).
[27]C. Oshima, T. Aizawa, M. Wuttig, R. Souda, S. Otani, Y. Ishizawa, H. Ishida, and K. Terakura, Phys. Rev. B **36**, 7510 (1987).
[28]M. Wuttig, C. Oshima, T. Aizawa, R. Souda, S. Otani, and Y. Ishizawa, Surf. Sci. **193**, 180 (1988).
[29]M. W. Finnis and V. Heine, J. Phys. F **4**, L37 (1974).
[30]U. Landman, R. N. Hill, and M. Mostoller, Phys. Rev. B **21**, 448 (1980).
[31]H. L. Davis and J. R. Noonan, Phys. Rev. Lett. **54**, 566 (1985); J. Vac. Sci. Technol. **A3**, 1507 (1985).
[32]J. R. Noonan and H. L. Davis, Science **234**, 310 (1986).
[33]J. R. Noonan and H. L. Davis, Phys. Rev. Lett. **59**, 1714 (1987).
[34]H. L. Davis and J. R. Noonan, in Vol. 83 of *Materials Research Society Symposium Proceedings,* edited by D. M. Zehner and G. W. Goodman (MRS, Pittsburgh, 1987), p. 3.
[35]S.-C. Lui, J. M. Mundenar, E. W. Plummer, M. Mostoller, R. M. Nicklow, D. M. Zehner, W. K. Ford, and J. Erskine, in Vol. 83 of *Materials Research Society Symposium Proceedings,* edited by D. M. Zehner and G. W. Goodman (MRS, Pittsburgh, 1987), p. 47.
[36]S. M. Yalisove and W. R. Graham, Surf. Sci. **183**, 556 (1987).
[37]D. R. Mullins, and S. H. Overbury, Surf. Sci. **199**, 141 (1988).
[38]H. Niehus, Nucl. Instrum. Methods B **33**, 876 (1988).
[39]R. Beyers, Ki Bum Kim, and R. Sinclair, J. Appl. Phys. **61**, 2195 (1987).
[40]T. Sands, Appl. Phys. Lett. **52**, 197 (1988).
[41]See, for example, J. R. D. Copley, R. W. Macpherson, and T. Timusk, Phys. Rev. **182**, 965 (1969).
[42]J. W. D. Connolly and K. H. Johnson, in *Electronic Density of States,* edited by L. H. Bennett, Nat. Bur. Stand. (U.S.) Spec. Publ. No. 323 (U. S. GPO, Washington, D. C., 1971), p. 19.
[43]D. J. Nagel, Ph.D. thesis, University of Maryland, 1977.
[44]See, for example, J. F. Cooke, J. W. Lynn, and H. L. Davis, Phys. Rev. B **21**, 4118 (1980).
[45]Debye temperatures depend on the thermal property they are derived from; the Debye temperatures corresponding to the rms displacements, for example, are not the same as those derived from the contributions to the specific heat.
[46]R. E. DeWames, T. Wolfram, and G. W. Lehman, Phys. Rev. **138**, A717 (1965).
[47]H. F. Bezdek and L. Feingold, Phys. Rev. B **4**, 1390 (1971).
[48]D. M. Zehner and G. R. Gruzalski, in Vol. 83 of *Materials Research Society Symposium Proceedings,* edited by D. M. Zehner and G. W. Goodman (MRS, Pittsburgh, 1987), p. 199.
[49]R. Franchy, M. Wuttig, and H. Ibach, Surf. Sci. **189/190**, 438 (1987).
[50]M. H. Kang and E. J. Mele, Phys. Rev. B **36**, 7371 (1987); in *The Structure of Surfaces II,* edited by J. F. van der Veen and M. A. Van Hove (Springer-Verlag, Berlin, 1987), p. 160.
[51]J. I. Lee, C. L. Fu, and A. J. Freeman, Phys. Rev. B **36**, 9318 (1987).
[52]S. P. Chen, A. F. Voter, and D. J. Srolovitz, Phys. Rev. Lett. **57**, 1308 (1986).
[53]K. M. Ho and K. P. Bohnen, Phys. Rev. Lett. **56**, 934 (1986).
[54]T. S. Rahman, J. E. Black, and D. L. Mills, Phys. Rev. B **25**, 883 (1982).